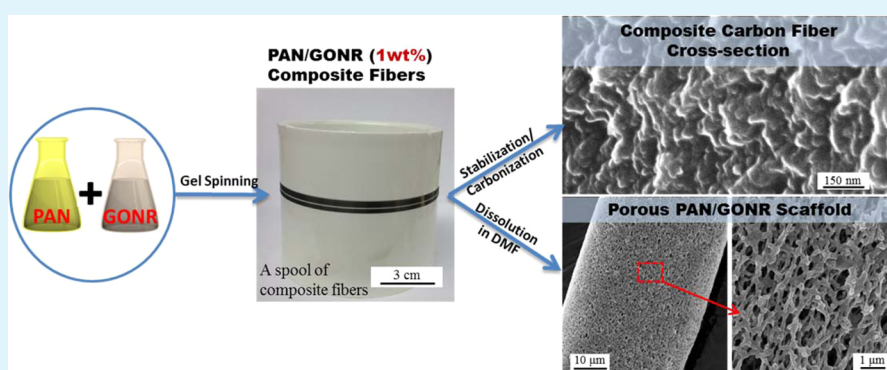# Polyacrylonitrile Fibers Containing Graphene Oxide Nanoribbons

An-Ting Chien,[†] H. Clive Liu,[†] Bradley A. Newcomb,[†] Changsheng Xiang,[‡] James M. Tour,[‡,§,#] and Satish Kumar*,[†]

[†]School of Materials Science and Engineering, Georgia Institute of Technology, 801 Ferst Drive, NW MRDC-1, Atlanta, Georgia 30332-0295, United States

[‡]Department of Chemistry, [§]Department of Materials Science and NanoEngineering, and [#]Smalley Institute for Nanoscale Science and Technology, Rice University, 6100 Main Street, Houston, Texas 77005, United States

Ⓢ Supporting Information

ABSTRACT: Graphene oxide nanoribbon (GONR) made by the oxidative unzipping of multiwalled carbon nanotube was dispersed in dimethylformamide and mixed with polyacrylonitrile (PAN) to fabricate continuous PAN/GONR composite fibers by gel spinning. Subsequently, PAN/GONR composite fibers were stabilized and carbonized in a batch process to fabricate composite carbon fibers. Structure, processing, and properties of the composite precursor and carbon fibers have been studied. This study shows that GONR can be used to make porous precursor and carbon fibers. In addition, GONR also shows the potential to make higher mechanical property carbon fibers than that achieved from PAN precursor only.

KEYWORDS: polyacrylonitrile, graphene oxide nanoribbon, fiber, carbon fiber

1. INTRODUCTION

Graphene nanoribbon (GNR) and graphene oxide nanoribbon (GONR) have a striplike structure with a high length-to-width ratio. GNR has the same flat sp^2 carbon honeycomb layered structure as graphene.[1,2] GONR with the similar oxygen-containing functional groups to graphene oxide are highly soluble in both water and polar solvents. GNR as well as GONR can be fabricated by a bottom-up synthesis method[3,4] or by unzipping or opening of carbon nanotubes (CNTs).[5−10] The unzipping direction can be controlled and GONRs can be produced directly.[9,10] The aspect ratio and uniformity of GNRs or GONRs can be controlled by the selection of CNT diameters and lengths. The GONRs can be used directly or further reduced to GNR for desired applications.[11] Various composites of GNRs and GONRs have been studied.[12−22] Polyacrylonitrile (PAN) fibers are currently the predominant precursors for carbon fiber.[23] CNT containing PAN fibers and PAN/CNT carbon fibers have been reported to expand the carbon fiber properties map.[24−26] Inclusion of GNR and GONR in PAN provides an alternative pathway for expanding the potential of PAN precursor fibers and the resulting carbon fibers. To date, spinning of continuous PAN/GNR or PAN/

GONR fibers has not been reported. Only electrospinning[13] of PAN/GNR composite nonwoven fibers has been reported in the literature. In this paper, we report the continuous production of PAN/GONR fibers by gel spinning. These fibers have been carbonized in the batch process. The effect of the presence of GONR on processing as well as structure and properties of the precursor as well as carbon fiber are discussed.

2. EXPERIMENTAL SECTION

PAN (homopolymer, viscosity average molecular weight: 2.5×10^5 g/mol) obtained from Japan Exlan Co. was dissolved in dimethylformamide (DMF from Sigma-Aldrich Co.). GONR fabricated from multiwalled carbon nanotube (MWCNT, Baytubes with a length of 0.2−1 μm and an outer diameter of 13 nm)[9,10,12] was obtained from Tour's group at Rice University. The SEM images of as-received GONR and the corresponding width distribution of GONR width are shown in Figure S1 of the Supporting Information and a transmission

electron micrograph of partially unzipped CNT is shown in Figure 1. GONR was dispersed in DMF by sonication and then
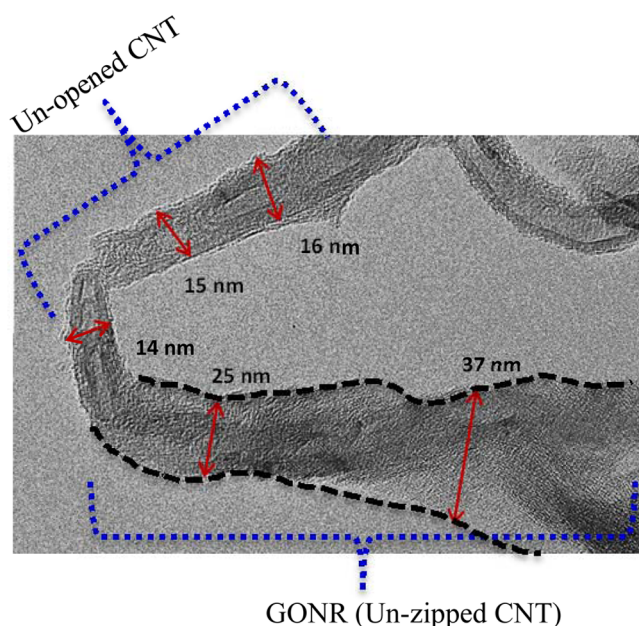
Figure 1. TEM image of partially unzipped CNT.

mixed with the PAN solution (at 1 wt % GONR concentration with respect to PAN). The UV−visible absorption spectra of GONR/DMF dispersion were obtained using UV−visible spectrometer (Lambda 35, Perkin-Elmer). The PAN/GONR composite and control PAN solutions were maintained at 70 °C before spinning. The fibers were gel-spun using a spinning unit manufactured by Hills, Inc. (Melbourne FL) and followed by two-stage drawing. First-stage drawing was carried out at room temperature, followed by second-stage drawing at 165 °C. The spinning condition and the draw ratios of different PAN/GONR fibers and the control PAN fibers are listed in Supporting Information, Table S1. The composite and control fibers are designated as G series and P series, respectively, with a lower case number representing the total draw ratio. The spin draw ratio is 3 for most composite and control fibers, except the fibers with a lower case letter s having a spin draw ratio equal to 1. The fibers were stabilized in air and carbonized in nitrogen at a nominal stress of 25 MPa in the furnace (Blue M Electric and MHI Inc.). The details of solution preparation, gel spinning, stabilization, and carbonization are given in the Supporting Information section.

Fiber bundles were embedded in epoxy resin (Epo-Fix, Electron Microscopy Sciences) and then sliced into 10−15 μm thick sections using a microtome (Leica, RM2255). These fiber cross sections were then observed using a scanning electron microscope (SEM, Zeiss Ultra60). Epoxy resin (Epo-Tek, Gatan, Inc.) was used to mount the PAN/GONR fibers on a copper 3-post Omniprobe lift-out grid (Electron Microscopy Sciences). Longitudinal fiber sections were etched by a focus ion beam (FIB) (FEI Nova Nanolab 200 FIB/SEM) at ion accelerating voltages of 30 and 5 kV. Samples were thinned until electron transparency was achieved and observed using a transmission electron microscope (TEM, FEI Tecnai F30), operated at 80 kV. As-received GONRs were also observed by TEM (JEOL JEM 100C), and the samples were prepared by slowly evaporating a drop of GONR suspension in DMF on an

amorphous carbon-coated copper grid at room temperature. The Raman spectra of composite fibers were collected using an optical microscope (Olympus BX41) and the XploRA system (HORIBA) using a 785 nm excitation laser with a polarizer and an analyzer parallel to each other. The composite fibers were placed parallel (0°) or perpendicular (90°) to the polarizer and analyzer during measurement.

Tensile properties were measured at a gauge length of 25.4 mm at a cross-head speed of 2 mm/min using Favimat (Textechno Herbert Stein GmbH & Co. KG.). Fiber diameters were calculated from their linear density, which was also measured with Favimat. The PAN density[27] was assumed to be 1.18 g/cm^3 and the carbon fiber density[23] was assumed to be 1.8 g/cm^3. Dynamic mechanical analysis was carried out using RSA III with frequencies of 0.1, 1, 10, and 80 Hz at a heating rate of 1 °C/min on a bundle of 100 filaments at 25.4 mm gage length. Wide-angle X-ray diffraction (WAXD) was conducted on fiber bundles using Cu Kα (λ = 0.1542 nm) on Rigaku Micromax-002. From the WAXD data, the structural parameters, including polymer crystallinity (X_c), crystal size (L) from equatorial scans, full-width at half-maximum (Z) from azimuthal scans, and the Herman's orientation factors (f), were determined according to previously described methods.[28−30]

3. RESULTS AND DISCUSSION

The UV−visible absorption spectra of GONR/DMF are given in Figure 2. The absorption peak at ∼280 nm is due to n−π^*
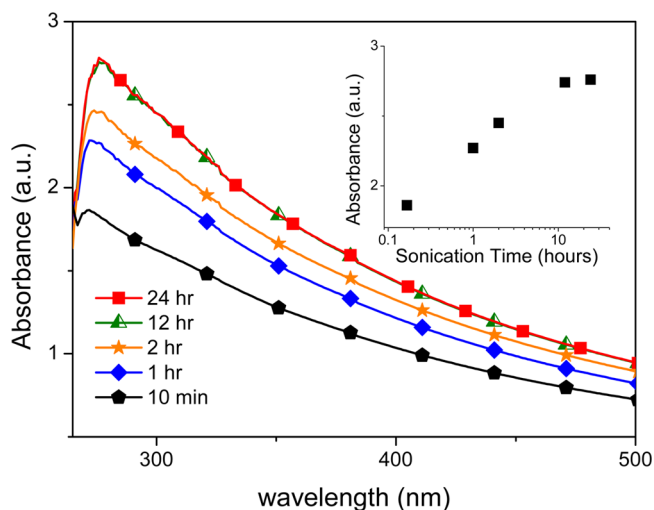

Figure 2. UV−visible absorption spectra of GONR dispersion in DMF with various sonication times. The inset figure shows the maximal absorption at 270−290 nm with various sonication times.

transition of C=O bond[31,32] in graphene oxide.[32−34] The absorbance increases with increase in sonication time. The increase in UV−visible absorption during the sonication process is also observed in carbon nanotube dispersions,[35] as well as carbon black dispersions.[36] The absorbance increases with increasing sonication time, and reached a plateau between 12 and 24 h of sonication. On the basis of this dispersion study, in the current work, GONR dispersion was sonicated for 24 h and then mixed with the PAN solution.

During spinning, the solid content of the PAN/GONR solution was higher, 18 g/100 mL, as compared to that for the control PAN solution, which was 15 g/100 mL. This is because the viscosity of the PAN/GONR solution with a solid content

of 15 g/100 mL was too low for spinning. Therefore, it became necessary to use a higher solid content for the composite fiber spinning. This difference in viscosity is an indicator of good interaction between PAN and GONR. Fiber spool and fiber cross sections are shown in Supporting Information, Figures S2 and S3. SEM image (Figure 3a) shows that the surface of the
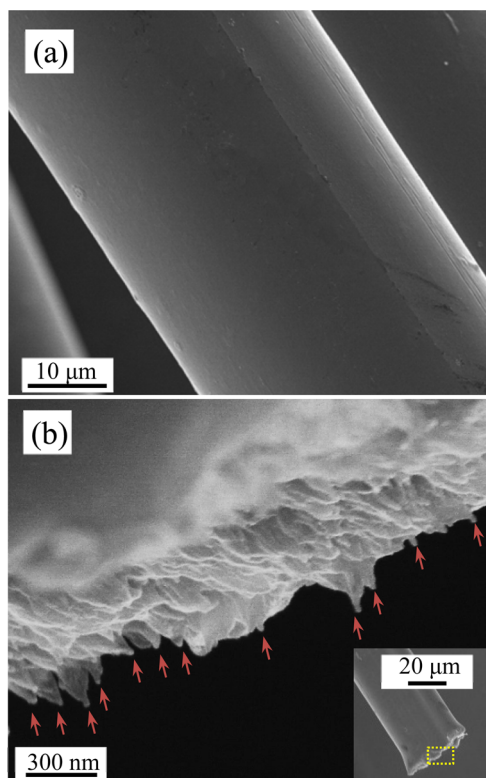
Figure 3. SEM images of (a) a fiber lateral surface of a G_{03} PAN/GONR composite fiber and (b) fractured surface with GONRs protruding from the surface indicated by arrows. The image of the fractured surface is taken from the broken fiber in the inset image.

G_{03} composite fiber is relatively smooth. SEM image (Figure 3b) of the fractured surface of the G_{03} composite fiber also shows the presence of GONRs, which appears to adhere reasonably well to PAN. The longitudinal section of G_{30} composite PAN/GONR fiber was observed in TEM after preparation using a focused ion beam. Figure S4 in the Supporting Information shows the presence of GONR (as dark gray strips) embedded in the polymer matrix and mostly aligned along the fiber axis direction.

To investigate PAN/GONR composite fiber structure, fiber G_{02s} (with a draw ratio of 2) was kept in DMF at room temperature for varying lengths of time (Figure 4a). Within minutes, fibers began to dissolve, and after about 7 min, the fiber broke. The broken fiber bundle floated in DMF and retained fibrous shape. The fiber remaining in DMF after 15 min exhibited porous structure (Figure 4b,c). This porous structure suggests a PAN-coated GONR network formed by the presence of only 1 wt % GONR. Strip width and void size distribution (Supporting Information, Figure S5) is determined from the SEM image in Figure 4c. The strip width was determined from the narrowest part of each strip. The strip width was in the range of 60−120 nm with an average width of about 90 nm. The width of original GONRs was about 40 nm, suggesting that about 20 nm thick polymer coating remained

on the GONRs in G_{02s} fiber after being immersed for 15 min in DMF at room temperature. A similar phenomenon has already been reported for polymer/CNT composite materials.[37,38] In addition, the porous structure consisted of voids of 200 nm to as large as 700 nm, and the average size was 394 ± 105 nm. The fiber pore size can be controlled by controlling fiber draw ratio, dissolution time, temperature, and the type of solvent. The porous PAN/GONR, PAN/GNR, and PAN/CNT fibers, as well as their carbonized porous products, may find applications in filtration, fuel cells, and capacitors.

PAN/GONR composite fibers G_{20s} (draw ratio = 20) were also placed in DMF at room temperature. However, these higher draw ratio composite fibers show higher resistance to the solvent than the lower draw ratio fibers. The G_{02s} composite fibers (draw ratio = 2) dissolved in DMF within 1 h, while G_{20s} composite fibers did not dissolve even after 1 week in DMF (Supporting Information, Figure S6a). Higher draw ratio improves the fiber structure such as increased crystallinity, crystal size, and molecular orientation, resulting in higher solvent resistance. However, we note that the control PAN fiber P_{20} (draw ratio = 20), without containing GONR, dissolved in DMF within a week (Supporting Information, Figure S6b). This further suggests that the presence of GONR changes the packing structure of PAN, rendering it insoluble in DMF.

Raman spectra of G_{30} composite fiber are given in Figure 5. The ratio between D and G peak intensities, which is denoted as I_D/I_G[39−41] and used as a measure of the quantity of ordered graphitic structure, is around 2.7. In addition, the peak intensity is much higher when the fiber was parallel to the polarization direction, suggesting high GONR orientation to the fiber axis.

The influence of GONRs on the fiber structure is investigated by analyzing two-dimensional WAXD, and the structural parameters of the fiber under various draw ratios are listed in Table 1. Generally, a higher draw ratio results in higher crystallinity (X_c), larger crystal size (L_c), and higher polymer chain orientation (f_{PAN}). In addition, GONRs in composite fibers also induce higher crystallinity and a larger crystal size. The orientation factor of PAN is also slightly increased, owing to the presence of GONRs. For example, G_{30} composite fibers exhibit crystallinity of 75% and a crystal size of 11 nm, which are 19% higher and 10% larger than the values from P_{30} control fibers. The orientation factor of PAN is also increased from 0.831 to 0.851.

The mechanical properties of composite and control fibers at various draw ratios are listed in Supporting Information, Table S2. The PAN/GONR fibers exhibit higher mechanical properties than the control PAN fibers. For example, G_{20s} composite fibers show tensile strength and modulus 35% and 18% higher than P_{20s} PAN fibers. At a draw ratio of 30, G_{30} PAN/GONR fiber exhibits tensile strength of 0.9 GPa and tensile modulus of 21.3 GPa with elongation at a break of 7.4%. The increased mechanical properties are a result of increased PAN crystallinity and orientation due to the presence of GONR.

Various fibers were also investigated for dynamic mechanical properties. Similar to the tensile properties, fibers with higher draw ratios and fibers with GONR show higher storage moduli, as compared to fibers with lower draw ratios and control fibers (Figure 6a,b). In addition, the plots of tan δ show typical β_c transition[42] in the range of 60−110 °C (Figure 6c,d). β_c transition is one of the thermo-mechanical transitions[24,42−44] for PAN, and this transition temperature is associated with the molecular motion from helical sequences in the para-crystalline
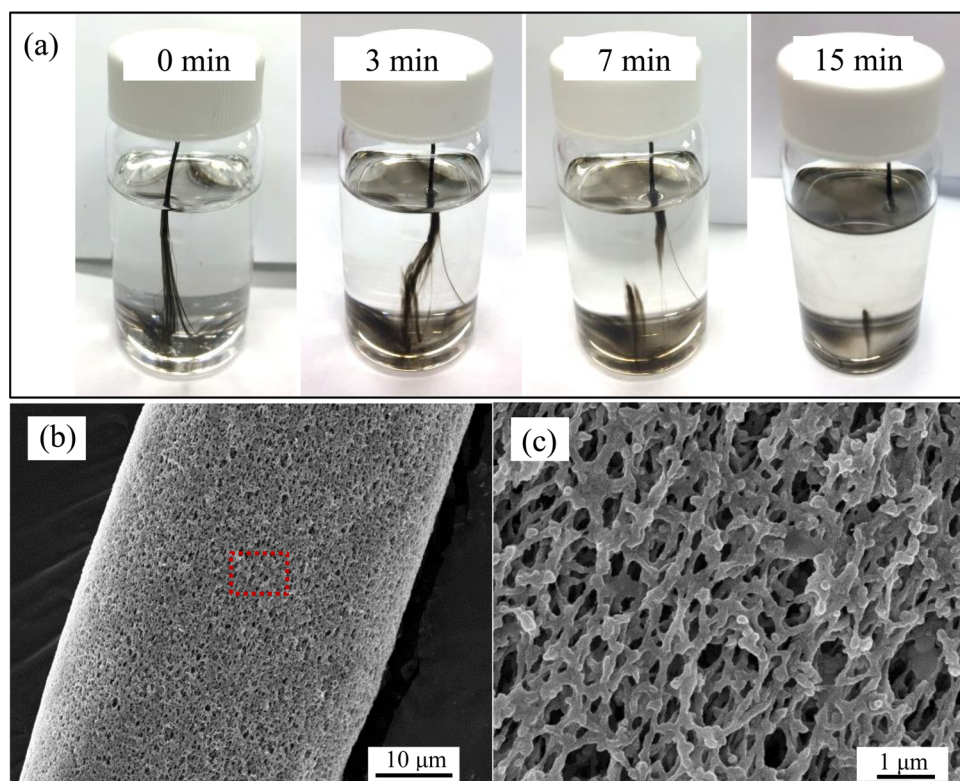
Figure 4. (a) G_{02s} PAN/GONR composite fibers after being placed in DMF for various lengths of time. (b) and (c) SEM images of G_{02s} PAN/GONR composite fibers after being placed in DMF for 15 min. (c) Higher magnification image of denoted region in (b).
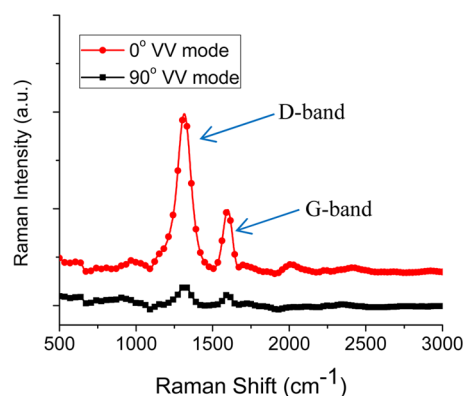
Figure 5. Raman spectra of G_{30} PAN/GONR composite fibers parallel (0°) and perpendicular (90°) to the polarization direction.

regions. Table S3 in the Supporting Information lists the β_c transition temperatures for composite and control fibers at various frequencies. The corresponding activation energies calculated using the Arrhenius equation are also listed in Supporting Information, Table S3. In general, when the draw ratio is increased, the β_c transition temperature decreases, and both the magnitude of the tan δ peak and the activation energy of the β_c relaxation are reduced. Using G_{15} and G_{30} as examples, the β_c transition temperature at 80 Hz is decreased from 93 to 80 °C, and the activation energy was reduced from 701 to 509 kJ/mol. This is because of the presence of more zigzag (and hence fewer helical) sequences at higher draw ratios.[42]

According to Figure 6d, GONRs also affect tan δ peak and slightly increased β_c transition temperature. Transition temperatures of the composite fibers are 3−8 °C higher than those of the control fibers under the same draw ratios (Supporting Information, Table S3), suggesting that GONRs can hinder or constrain the mobility of PAN polymer chains. The activation energy indicates the same influence and shows a higher value for the composite fibers (Supporting Information, Table S3). The composite fibers also showed a slight decrease in the magnitude of the tan δ peak. Considering the β_c transition represents the molecular motion of helical sequences, and since the existence of GONRs induced more zigzag structure as a result of the closer packing structure and decreased meridional 2θ peak position (Table 1), more stretched polymer chains and hence less helical structure was induced in the composite fibers. Therefore, the magnitude of tan δ is decreased in Figure 6d. The above phenomenon is similar to the influence of CNT[24] on PAN composite fibers, suggesting that GONRs have somewhat similar influence on polymer chains.

Composite (G_{30}) and control PAN fibers (P_{30}) with the highest draw ratios were selected for stabilization and carbonization. A bundle of fibers was stabilized under a stress of 25 MPa in air at 270 °C for 400 min and then at 315 °C for another 15 min. Stabilized fibers were subsequently carbonized in nitrogen at 1000, 1200, and 1300 °C for 5 min. Fibers with different stabilization and carbonization processes are summarized in Table 2. Figure S9 in the Supporting Information shows SEM images of the fracture surface of the composite carbon fiber. During carbonization, GONR is reduced to GNR.[13]

Stabilized and carbonized fibers were also investigated using WAXD (Supporting Information, Figure S10). During the stabilization process, PAN structure is converted to ladder structure, and subsequently transformed into turbostratic graphite-like structure[45,46] during carbonization process.[23,30] Typical diffraction peaks of PAN (at $2\theta \sim 17°$ and 30°) disappear after stabilization and carbonization processes, and the diffraction peaks of carbon ladder (at $2\theta \sim 26°$) and

Table 1. Structural Parameters of PAN/GONR Composite and Control PAN Fibers

sample	effective diameter[a] (μm)	PAN structural parameters					
		$X_c{}^b$ (%)	$L_{PAN}{}^c$ (nm)	$f_{PAN}{}^d$	$d_{2\theta\sim17°}{}^e$ (nm)	$d_{2\theta\sim30°}{}^f$ (nm)	$2\theta_{meridional}{}^g$ (deg)
		PAN/GONR Composite Fibers					
G$_{30}$	13.0 ± 0.7	75	11.0	0.851	0.520	0.301	38.9
G$_{20}$	15.1 ± 0.7	69	9.4	0.828	0.522	0.302	39.1
G$_{15}$	16.7 ± 1.6	56	9.2	0.800	0.524	0.303	39.2
G$_{03}$	38.6 ± 0.4	51	2.9	0.264	0.522	0.315	39.9
G$_{20s}$	15.6 ± 0.8	57	10.9	0.847	0.523	0.302	39.1
G$_{02s}$	48.7 ± 1.1	47	3.2	0.372	0.525	0.307	39.7
		Control PAN Fibers					
P$_{30}$	11.1 ± 0.6	63	10.0	0.831	0.521	0.302	38.9
P$_{20}$	14.3 ± 1.0	57	9.2	0.817	0.524	0.302	38.8
P$_{15}$	16.0 ± 0.9	56	9.2	0.794	0.524	0.303	39.0
P$_{20s}$	15.6 ± 1.6	52	10.5	0.847	0.523	0.303	39.1
P$_{02s}$	49.4 ± 4.0	46	3.5	0.320	0.528	0.306	39.8

[a]Effective diameters of fibers were calculated from the linear density obtained by Favimat and the density of PAN (1.18 g/cm³). [b]X_c: crystallinity from integrated radial scans. [c]L_{PAN}: crystal size ($2\theta \sim 17°$) according to Scherrer's equation with $K = 0.9$. [d]f_{PAN}: orientation factor of PAN polymer chains. [e]$d_{2\theta}$: d-spacing for $2\theta \sim 17°$. [f]$d_{2\theta}$: d-spacing for $2\theta \sim 30°$. [g]$2\theta_{meridional}$: meridional peak position.
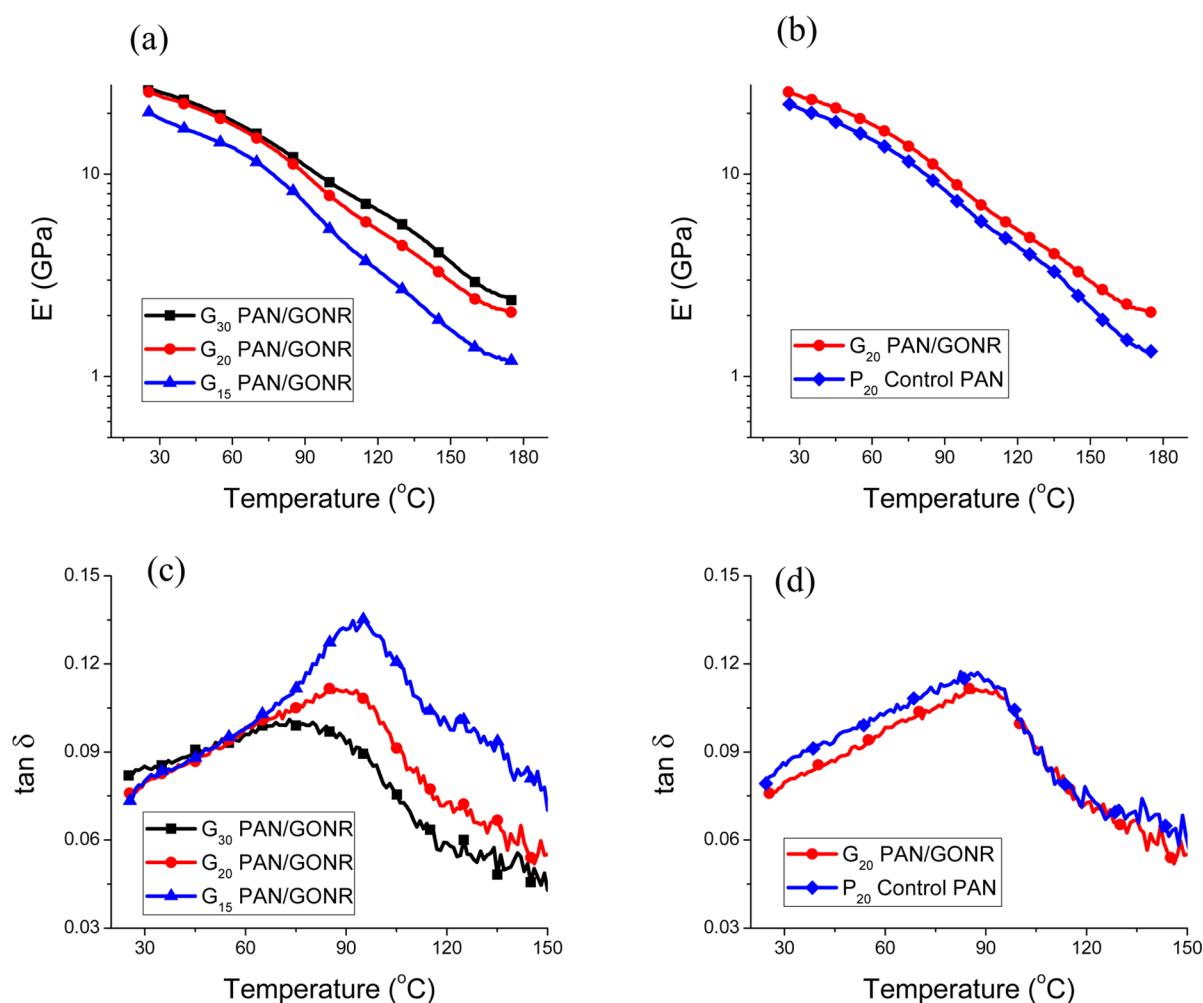

Figure 6. Dynamic mechanical storage modulus (a and b) and tan δ (c and d) plots for PAN/GONR composite and PAN control fibers as a function of temperature at a frequency of 10 Hz.

turbostratic carbon structure (at $2\theta \sim 26°$ and $43°$) occur for stabilized and carbonized fibers.

Structural parameters of various stabilized and carbonized fibers are listed in Table 2. A comparison between PAN/GONR and PAN based carbon fibers suggest moderate improvement in PAN/GONR carbon fiber structure, as compared to the PAN carbon fiber structure. Similarly, carbonized composite fibers exhibit somewhat better mechan-

Table 2. Structural Parameters of Stabilized and Carbonized PAN/GONR and PAN Fibers

sample	description (holding temperature/time)	f_{Ladder} [a] (%)	Z_{Ladder} [b] (deg)	$d_{2\theta\sim26°}$ [c] (nm)	$L_{2\theta\sim26°}$ [d] (nm)	$L_{2\theta\sim43°}$ [d] (nm)
		Stabilized Fibers				
		structural parameters				
		PAN/GONR Composite Fibers (G$_{30}$)				
GS$_1$	(1) 270 °C/400 min; (2) 320 °C/15 min	0.449	45.6	3.399	1.1	1.2
		PAN Fibers (P$_{30}$)				
S$_1$	(1) 270 °C/400 min; (2) 320 °C/15 min	0.418	46.7	3.433	1.1	1.2

sample	description (holding temperature/time)	$f_{(002)}$ [a] (%)	$Z_{(002)}$ [b] (deg)	$d_{2\theta\sim26°}$ [c] (nm)	$L_{2\theta\sim26°}$ [d] (nm)	$L_{2\theta\sim43°}$ [d] (nm)
		Carbonized Fibers				
		structural parameters				
		PAN/GONR Composite Fibers (G$_{30}$)				
GC$_1$	1300 °C/5 min	0.684	29.3	3.492	1.5	1.9
GC$_2$	1200 °C/5 min	0.682	29.5	3.496	1.3	1.7
GC$_3$	1000 °C/5 min	0.687	30.0	3.499	1.2	1.4
GC$_4$	1300 °C/50 min	0.689	29.9	3.501	1.5	2.0
		PAN Fibers (P$_{30}$)				
C$_1$	1300 °C/5 min	0.673	30.7	3.518	1.2	1.8
C$_2$	1200 °C/5 min	0.679	29.7	3.520	1.3	1.4
C$_3$	1000 °C/5 min	0.678	30.1	3.516	1.1	1.4

[a]f: orientation factor of stabilized ladder structure and carbonized turbostratic (002) plane. [b]Z: Full-width at half-maximum (fwhm) from azimuthal scans of a stabilized ladder structure and carbonized graphite (002) plane at $2\theta \sim 26°$. [c]$d_{2\theta\sim26}$: d-spacing for peak at $2\theta \sim 26°$. [d]L: crystal size ($2\theta \sim 26°$ and $2\theta \sim 43°$) according to Scherrer's equation with $K = 0.9$.

ical properties than control fibers (Table 3). Table 3 also shows the influence of carbonization temperature on mechanical

Table 3. Mechanical Properties of Carbonized PAN/GONR Composite Fibers

sample	effective diameter[a] (μm)	tensile strength (GPa)	tensile modulus (GPa)	elongation at break (%)
	Carbonized PAN/GONR Composite Fibers (G$_{30}$)			
GC$_1$	6.8 ± 0.4	1.62 ± 0.24	230 ± 9	0.66 ± 0.11
GC$_2$	7.0 ± 0.3	1.82 ± 0.38	229 ± 9	0.79 ± 0.20
GC$_3$	7.3 ± 0.5	1.72 ± 0.26	196 ± 5	0.84 ± 0.16
GC$_4$	6.8 ± 0.3	1.17 ± 0.20	232 ± 6	0.49 ± 0.10
	Carbonized PAN Fibers (P$_{30}$)			
C$_1$	6.5 ± 0.5	1.58 ± 0.23	222 ± 7	0.72 ± 0.10
C$_2$	7.3 ± 0.7	1.56 ± 0.21	203 ± 7	0.75 ± 0.10
C$_3$	7.8 ± 0.7	1.64 ± 0.22	184 ± 10	0.86 ± 0.15

[a]Effective diameters of the fibers were calculated from linear density measured by Favimat and the density of carbon fiber (1.8 g/cm^3).

properties. Higher carbonization temperature results in a larger $L_{2\theta\sim26°}$ and $L_{2\theta\sim43°}$ crystal size of the PAN and PAN/GONR based carbon fibers, corresponding to increased tensile moduli of both the composite and control fibers when carbonized at higher temperatures. For example, GC$_1$ fibers (carbonized at 1300 °C) exhibit tensile modulus of 230 GPa, which is 17% higher than the value of GC$_3$ fibers (carbonized at 1000 °C).

4. CONCLUSION

The gel-spinning method was used to successfully fabricate PAN/GONR composite fibers with 1 wt % GONRs in the polymer. GONRs influenced the structure of PAN and induced higher polymer crystallinity, and higher mechanical properties in the fiber. PAN/GONR fibers exhibited higher solvent resistance than PAN fibers of the same draw ratio. This study also provides a pathway for making porous polymer/GONR, polymer/GNR, and polymer/CNT fibers, as well as porous carbon fibers of controlled porosity. It is also demonstrated that carbonized PAN/GONR fibers can exhibit higher mechanical properties than the corresponding carbonized PAN fiber.

■ ASSOCIATED CONTENT

$\mathbf{S}$ Supporting Information

Details of the fabrication process including solution preparation, gel spinning, stabilization, and carbonization, mechanical properties and dynamic mechanical analysis results of PAN/GONR and PAN fibers, micrograph of PAN/GONR fibers, SEM images of as-received GONRs, fiber cross section of PAN/GONR fibers, and composite carbon fibers, TEM image of longitudinal section of PAN/GONR fibers, strip width and void size distributions of porous PAN/GONR fibers, and WAXD diffraction patterns of composite fibers before and after stabilization and carbonization. This material is available free of charge via the Internet at http://pubs.acs.org.

■ AUTHOR INFORMATION

Corresponding Author
*E-mail: Satish.Kumar@mse.gatech.edu. Phone: 404-894-7550. Fax: 404-894-8780.

Notes
The authors declare no competing financial interest.

■ ACKNOWLEDGMENTS

■ REFERENCES

(1) Terrones, M.; Botello-Mendez, A. R.; Campos-Delgado, J.; Lopez-Urias, F.; Vega-Cantu, Y. I.; Rodriguez-Macias, F. J.; Elias, A. L.; Munoz-Sandoval, E.; Cano-Marquez, A. G.; Charlier, J.-C.; Terrones, H. Graphene and graphite nanoribbons: Morphology, Properties, Synthesis, Defects and Applications. *Nano Today* **2010**, *5*, 351−372.

(2) Kim, H.; Abdala, A. A.; MacOsko, C. W. Graphene/Polymer Nanocomposites. *Macromolecules* **2010**, *43*, 6515−6530.

(3) Campos-Delgado, J.; Romo-Herrera, J. M.; Jia, X. T.; Cullen, D. A.; Muramatsu, H.; Kim, Y. A.; Hayashi, T.; Ren, Z. F.; Smith, D. J.; Okuno, Y.; Ohba, T.; Kanoh, H.; Kaneko, K.; Endo, M.; Terrones, H.; Dresselhaus, M. S.; Terrones, M. Bulk Production of a New Form of Sp² Carbon: Crystalline Graphene Nanoribbons. *Nano Lett.* **2008**, *8*, 2773−2778.

(4) Cai, J. M.; Ruffieux, P.; Jaafar, R.; Bieri, M.; Braun, T.; Blankenburg, S.; Muoth, M.; Seitsonen, A. P.; Saleh, M.; Feng, X. L.; Mullen, K.; Fasel, R. Atomically Precise Bottom-up Fabrication of Graphene Nanoribbons. *Nature* **2010**, *466*, 470−473.

(5) Terrones, M. Materials Science: Nanotubes Unzipped. *Nature* **2009**, *458*, 845−846.

(6) Cano-Marquez, A. G.; Rodriguez-Macias, F. J.; Campos-Delgado, J.; Espinosa-Gonzalez, C. G.; Tristan-Lopez, F.; Ramirez-Gonzalez, D.; Cullen, D. A.; Smith, D. J.; Terrones, M.; Vega-Cantu, Y. I. Ex-MWNTs: Graphene Sheets and Ribbons Produced by Lithium Intercalation and Exfoliation of Carbon Nanotubes. *Nano Lett.* **2009**, *9*, 1527−1533.

(7) Elias, A. L.; Botello-Mendez, A. R.; Meneses-Rodriguez, D.; Gonzalez, V. J.; Ramirez-Gonzalez, D.; Ci, L.; Munoz-Sandoval, E.; Ajayan, P. M.; Terrones, H.; Terrones, M. Longitudinal Cutting of Pure and Doped Carbon Nanotubes to Form Graphitic Nanoribbons Using Metal Clusters as Nanoscalpels. *Nano Lett.* **2010**, *10*, 366−372.

(8) Jiao, L.; Li, Z.; Xinran, W.; Diankov, G.; Hongjie, D. Narrow Graphene Nanoribbons From Carbon Nanotubes. *Nature* **2009**, *458*, 877−880.

(9) Kosynkin, D. V.; Higginbotham, A. L.; Sinitskii, A.; Lomeda, J. R.; Dimiev, A.; Price, B. K.; Tour, J. M. Longitudinal Unzipping of Carbon Nanotubes to Form Graphene Nanoribbons. *Nature* **2009**, *458*, 872−876.

(10) Higginbotham, A. L.; Kosynkin, D. V.; Sinitskii, A.; Sun, Z. Z.; Tour, J. M. Lower-Defect Graphene Oxide Nanoribbons from Multiwalled Carbon Nanotubes. *ACS Nano* **2010**, *4*, 2059−2069.

(11) Xiang, C. S.; Behabtu, N.; Liu, Y. D.; Chae, H. G.; Young, C. C.; Genorio, B.; Tsentalovich, D. E.; Zhang, C. G.; Kosynkin, D. V.; Lomeda, J. R.; Hwang, C. C.; Kumar, S.; Pasquali, M.; Tour, J. M. Graphene Nanoribbons as an Advanced Precursor for Making Carbon Fiber. *ACS Nano* **2013**, *7*, 1628−1637.

(12) Rafiee, M. A.; Lu, W.; Thomas, A. V.; Zandiatashbar, A.; Rafiee, J.; Tour, J. M.; Koratkar, N. A. Graphene Nanoribbon Composites. *ACS Nano* **2010**, *4*, 7415−7420.

(13) Matsumoto, H.; Imaizumi, S.; Konosu, Y.; Ashizawa, M.; Minagawa, M.; Tanioka, A.; Lu, W.; Tour, J. M. Electrospun Composite Nanofiber Yarns Containing Oriented Graphene Nanoribbons. *ACS Appl. Mater. Interfaces* **2013**, *5*, 6225−6231.

(14) Liu, M. K.; Zhang, C.; Tjiu, W. W.; Yang, Z.; Wang, W. Z.; Liu, T. X. One-Step Hybridization of Graphene Nanoribbons with Carbon Nanotubes and Its Strong-yet-Ductile Thermoplastic Polyurethane Composites. *Polymer* **2013**, *54*, 3124−3130.

(15) Wang, J. L.; Shi, Z. X.; Ge, Y.; Wang, Y.; Fan, J. C.; Yin, J. Functionalization of Unzipped Carbon Nanotube via In Situ Polymerization for Mechanical Reinforcement of Polymer. *J. Mater. Chem.* **2012**, *22*, 17663−17670.

(16) Fan, J. C.; Shi, Z. X.; Tian, M.; Wang, J. L.; Yin, J. Unzipped Multiwalled Carbon Nanotube Oxide/Multiwalled Carbon Nanotube Hybrids for Polymer Reinforcement. *ACS Appl. Mater. Interfaces* **2012**, *4*, 5956−5965.

(17) Fan, J. C.; Shi, Z. X.; Ge, Y.; Wang, Y.; Wang, J. L.; Yin, J. Mechanical Reinforcement of Chitosan Using Unzipped Multiwalled Carbon Nanotube Oxides. *Polymer* **2012**, *53*, 657−664.

(18) Wang, Y.; Shi, Z. X.; Yin, J. Unzipped Multiwalled Carbon Nanotubes for Mechanical Reinforcement of Polymer Composites. *J. Phys. Chem. C* **2010**, *114*, 19621−19628.

(19) Xiang, C. S.; Lu, W.; Zhu, Y.; Sun, Z. Z.; Yan, Z.; Hwang, C. C.; Tour, J. M. Carbon Nanotube and Graphene Nanoribbon-Coated Conductive Kevlar Fibers. *ACS Appl. Mater. Interfaces* **2012**, *4*, 131−136.

(20) Joshi, A.; Bajaj, A.; Singh, R.; Alegaonkar, P. S.; Balasubramanian, K.; Datar, S. Graphene Nanoribbon-PVA Composite as EMI Shielding Material in the X Band. *Nanotechnology* **2013**, *24*, 455705.

(21) Volman, V.; Zhu, Y.; Raji, A.-R. O.; Genorio, B.; Lu, W.; Xiang, C.; Kittrell, C.; Tour, J. M. Radio-Frequency-Transparent, Electrically Conductive Graphene Nanoribbon Thin Films as Deicing Heating Layers. *ACS Appl. Mater. Interfaces* **2014**, *6*, 298−304.

(22) Min, L.; Jinchen, F.; Zixing, S.; Hong, L.; Jie, Y. Kevlar-Functionalized Graphene Nanoribbon for Polymer Reinforcement. *Polymer* **2014**, *55*, 2578−87.

(23) Liu, Y. D.; Kumar, S. Recent Progress in Fabrication, Structure, and Properties of Carbon Fibers. *Polym. Rev.* **2012**, *52*, 234−258.

(24) Chae, H. G.; Minus, M. L.; Kumar, S. Oriented and Exfoliated Single Wall Carbon Nanotubes in Polyacrylonitrile. *Polymer* **2006**, *47*, 3494−3504.

(25) Liu, Y. D.; Chae, H. G.; Kumar, S. Gel-Spun Carbon Nanotubes/Polyacrylonitrile Composite Fibers. Part I: Effect of Carbon Nanotubes on Stabilization. *Carbon* **2011**, *49*, 4466−4476.

(26) Chien, A.-T.; Gulgunje, P. V.; Chae, H. G.; Joshi, A. S.; Moon, J.; Feng, B.; Peterson, G. P.; Kumar, S. Functional Polymer-Polymer/Carbon nanotube Bi-Component Fibers. *Polymer* **2013**, *54*, 6210−6217.

(27) Masson, J. C. *Acrylic Fiber Technology and Applications*; Marcel Dekker: New York, 1995.

(28) Chae, H. G.; Sreekumar, T. V.; Uchida, T.; Kumar, S. A Comparison of Reinforcement Efficiency of Various Types of Carbon Nanotubes in Polyacrylonitrile Fiber. *Polymer* **2005**, *46*, 10925−10935.

(29) Sreekumar, T. V.; Liu, T.; Min, B. G.; Guo, H.; Kumar, S.; Hauge, R. H.; Smalley, R. E. Polyacrylonitrile Single-Walled Carbon Nanotube Composite Fibers. *Adv. Mater.* **2004**, *16*, 58−61.

(30) Chae, H. G.; Minus, M. L.; Rasheed, A.; Kumar, S. Stabilization and Carbonization of Gel Spun Polyacrylonitrile/Single Wall Carbon Nanotube Composite Fibers. *Polymer* **2007**, *48*, 3781−3789.

(31) Chen, Y.; Zhuang, Q. X.; Liu, X. Y.; Liu, J.; Lin, S. L.; Han, Z. W. Preparation of Thermostable PBO/Graphene Nanocomposites with High Dielectric Constant. *Nanotechnology* **2013**, *24*, 245702.

(32) Luo, Z. T.; Lu, Y.; Somers, L. A.; Johnson, A. T. C. High Yield Preparation of Macroscopic Graphene Oxide Membranes. *J. Am. Chem. Soc.* **2009**, *131*, 898−899.

(33) Sun, Z. Z.; Yan, Z.; Yao, J.; Beitler, E.; Zhu, Y.; Tour, J. M. Growth of graphene from solid carbon sources. *Nature* **2010**, *468*, 549−552.

(34) Liu, Z. B.; Xu, Y. F.; Zhang, X. Y.; Zhang, X. L.; Chen, Y. S.; Tian, J. G. Porphyrin and Fullerene Covalently Functionalized Graphene Hybrid Materials with Large Nonlinear Optical Properties. *J. Phys. Chem. B* **2009**, *113*, 9681−9686.

(35) Yu, J. R.; Grossiord, N.; Koning, C. E.; Loos, J. Controlling the Dispersion of Multi-Wall Carbon Nanotubes in Aqueous Surfactant Solution. *Carbon* **2007**, *45*, 618−623.

(36) Sh, M. S.; Fard, F. G.; Khatibi, E.; Sarpoolaky, H. Dispersion and Stability of Carbon Black Nanoparticles, Studied by Ultraviolet-Visible Spectroscopy. *J. Taiwan Inst. Chem. Eng.* **2009**, *40*, 524−527.

(37) Jain, R.; Minus, M. L.; Chae, H. G.; Kumar, S. Processing, Structure, and Properties of PAN/MWNT Composite Fibers. *Macromol. Mater. Eng.* **2010**, *295*, 742−749.

(38) Zhang, Y.; Song, K.; Meng, J.; Minus, M. L. Tailoring Polyacrylonitrile Interfacial Morphological Structure by Crystallization in the Presence of Single-Wall carbon Nanotubes. *ACS Appl. Mater. Interfaces* **2013**, *5*, 807−814.

(39) Cancado, L. G.; Jorio, A.; Ferreira, E. H. M.; Stavale, F.; Achete, C. A.; Capaz, R. B.; Moutinho, M. V. O.; Lombardo, A.; Kulmala, T. S.; Ferrari, A. C. Quantifying Defects in Graphene via Raman Spectroscopy at Different Excitation Energies. *Nano Lett.* **2011**, *11*, 3190−3196.

(40) Eckmann, A.; Felten, A.; Verzhbitskiy, I.; Davey, R.; Casiraghi, C. Raman Study on Defective Graphene: Effect of the Excitation Energy, Type, and Amount of Defects. *Phys. Rev. B* **2013**, *88*, 035426.

(41) Ferreira, E. H. M.; Moutinho, M. V. O.; Stavale, F.; Lucchese, M. M.; Capaz, R. B.; Achete, C. A.; Jorio, A. Evolution of the Raman Spectra from Single-, Few-, and Many-Layer Graphene with Increasing Disorder. *Phys. Rev. B* **2010**, *82*, 125429.

(42) Sawai, D.; Kanamoto, T.; Yamazaki, H.; Hisatani, K. Dynamic Mechanical Relaxations in Poly(acrylonitrile) with Different Stereoregularities. *Macromolecules* **2004**, *37*, 2839−2846.

(43) Bashir, Z. The Hexagonal Mesophase in Atactic Polyacrylonitrile: A New Interpretation of the Phase Transitions in the Polymer. *J. Macromol. Sci., Part B: Phys.* **2001**, *B40*, 41−67.

(44) Kimmel, R. M.; Andrews, R. D. Birefringence Effects in Acrylonitrile Polymers. II. The Nature of the 140°C Transition. *J. Appl. Phys.* **1965**, *36*, 3063.

(45) Edie, D. D. The Effect of Processing on the Structure and Properties of Carbon Fibers. *Carbon* **1998**, *36*, 345−362.

(46) Fujimoto, H. Theoretical X-ray Scattering Intensity of Carbons with Turbostratic Stacking and AB Stacking Structures. *Carbon* **2003**, *41*, 1585−1592.